DOI 10.1007/s10946-024-10189-3
Journal of Russian Laser Research, Volume 45, Number 1, January, 2024

STABLE ULTRASHORT PULSE GENERATION USING A COILED AND TAPERED FEW-MODE-FIBER POLARIZATION CONTROLLER AS A SATURABLE ABSORBER

F. Y. Zhao,[1] X. H. Hu,[2*] F. M. Zou,[1] T. Zhang,[2] Y. S. Wang,[2] and J. Q. Lan[1]

[1] *School of Electronic, Electrical Engineering and Physics*
Fujian University of Technology
Fujian 350118, China

[2] *State Key Laboratory of Transient Optics and Photonics*
Xi'an Institute of Optics and Precision Mechanics, Chinese Academy of Sciences
Xi'an 710119, China

*Corresponding author e-mail: xhhu@opt.ac.cn

Abstract

We present a coiled and tapered graded-index few-mode-fiber (FMF) polarization controller (PC) as a saturable absorber (SA) in an all-fiber laser. We obtain the 845 fs ultrashort pulse with a signal-to-noise ratio (SNR) of 65 dB, using a tapered graded-index FMF of 40 cm in the cavity. The spectrum is centered at 1588.2 nm with a 3 dB spectral bandwidth of 4.04 nm. Furthermore, a *Q*-switched mode-locked state is observed between 140 and 360 mW of the pump power in the cavity. The results further demonstrate the application of a coiled and tapered graded-index FMF PC as a SA for stable high-energy ultrashort pulse formation and provide a technical method for generating ultrashort pulses.

Keywords: fiber laser, mode-locked graded-index few-mode fiber, saturable absorber.

1. Introduction

In recent years, passively mode-locked fiber lasers (MLFLs) have attracted considerable attention due to their intense applications in optical sensing, communications, micromachining, and medicine [1–3]. Passive saturable absorbers (SAs) are essential elements that trigger a pulsed regime in lasers. Various types of SAs have been adopted for ultrashort pulse generation in passively MLFLs, such as semiconductor SA mirrors (SESAMs) [4,5] and nanomaterials, including predominantly Carbon nanotubes (CNTs) [6,7], Graphene [8–10], Black Phosphorus (BP) [11–13], and transition metal dichalcogenides (TMDs) [14–16]. Multimode interference (MMI)-based SAs are preferred for fiber lasers because of their all-fiber structure over a broad wavelength range.

In 2013, Mafi et al. proposed an MMI-SA sandwiched between two segments of single-mode fibers (SMFs) [17]. A precise adjustment of the MMI length is difficult to achieve because of the short imaging length of MMI. In 2017, Wang et al. experimentally demonstrated mode-locking operation at the 1.5 μm waveband by placing a short-length step-index multimode fiber (SIMF) ahead of a graded-index multimode fiber (GIMF) for the first time [18]. The same year, researchers reported the soliton generation in a fiber laser doped with Ytterbium (Yb) and Thulium (Tm), using the same SA structure [19, 20]. We developed a stretched pulse laser and a higher energy conventional soliton at the 1.5 μm waveband

Manuscript submitted by the authors in English on December 9, 2023.

with the same structure [21, 22]. Later, researchers reported ultrashort pulse generation by combining non-core fiber (NCF) and GIMFs in a fiber laser [23]. High-energy conventional and dissipative soliton generations were verified in an Erbium (Er)-doped fiber laser, using a GIMF modulator to average the output power [24]. A few-mode-fiber (FMF)-based SA that operates on the principle of the MMI effect was proposed to develop an all-fiber femtosecond mode-locked Yb laser [25]. Then, a tunable mode-locked Yb-doped fiber laser was reported based on the nonlinear Kerr beam clean-up effect. Dissipative soliton pulses with a tunable central wavelength can be obtained by adjusting the bending condition of GIMF [26]. Recently, a tapered GIMF as an effective SA was adopted to achieve mode-locking operation. Later, a Graphene film and ZnO coating acting with tapered GIMF as the SA were investigated in the experiment [27, 28]. However, a tapered GIMF is fragile and can easily break during experiments.

In this paper, for the first time up to our knowledge, we propose and experimentally demonstrate a coiled and tapered few-mode-fiber polarization-controlled SA. Using the SA, we obtain the conventional soliton operation under a threshold pump power of 370 mW. The pulse spectrum is centered at 1588.2 nm, with a 3 dB spectral bandwidth of 4.04 nm. In the experiment, we obtain a pulse duration of 845 fs. Owing to the merits of all-fiber-structure SA, the SNR of the radio frequency spectrum can reach 65 dB; also, the fiber laser exhibits high stability.

2. Saturable Absorber

The FMF is tapered by equipment of Fujikura FSM-100 and LZM-100, the diameter of which is tapered from 125 to 110 μm. The purpose of tapered FMF in the fiber laser is to change the mode field distribution and excite higher-order modes. Hence, a large number of modes travel in the FMF along different paths, changing the self-imaging period. Furthermore, the tapered FMF is coiled on the paddles of the polarization controller (PC). The intensity is periodically modulated by tuning the paddles, producing an effective SA, without precisely controlling the length of the FMF [29]. We adjust the polarization state of the PC with different higher-order modes to achieve the mode diameter ratio in order to produce an effective SA.

We measure the nonlinear characteristics, using the balanced twin-detector measurement technique in order to investigate the tapered FMF SA as a mode-locking element. In our experiment, the light source is a figure-of-nine cavity mode-locked laser; the center wavelength is 1563 nm, the 3 dB spectrum bandwidth is 50 nm, the repetition frequency is 103.7 MHz, and the pulse width is 500 fs. The nonlinear absorption characteristics of a coiled and tapered FMF-based PC as an SA are relevant. In Fig. 1, we present the nonlinear SA curve from our experiment. The modulated depth (MD) is 4.1%, an advantage when designing the mode-locked pulses in lasers. The saturation intensity is estimated to be 9.59 MW/cm^2.

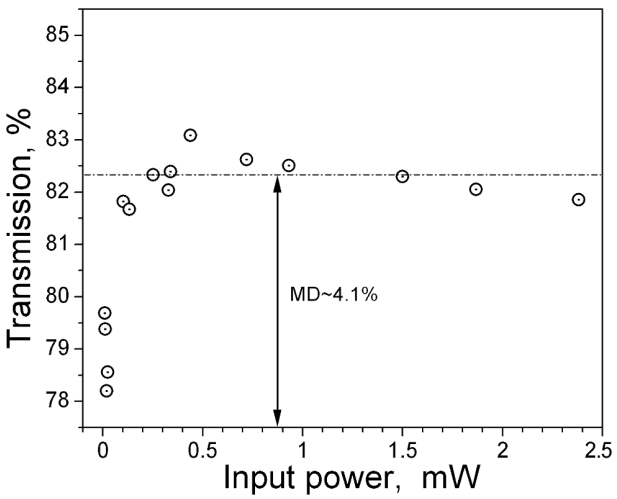

Fig. 1. Nonlinear characteristics curve of coiled and tapered FMF-based PC as an SA.

3. Experimental Setup

In Fig. 2, we illustrate the schematic of the passively mode-locked Er-doped fiber laser. The ring cavity is pumped by a 980 nm laser diode (LD) light source with a maximum pump power of 700 mW. The pump light is coupled into the laser, using a 980/1550 nm wavelength division multiplexer (WDM). As the gain medium, we use a 2.7 m Er-doped fiber (EDF, Nufern 7–125) with a group velocity dispersion (GVD) of – 42 ps/nm/km. A 40 cm tapered FMF (Changfei, GI-6 mode), with GVD of 22 ps/nm/km, is fused in the cavity. The passive component is a standard SMF with a GVD of 18 ps/nm/km. The total length of the cavity is estimated to be 8.15 m. Therefore, the net dispersion is managed with anomalous dispersion to form a conventional soliton. A PC is used to precisely tune the linear birefringence and intensity of the cavity. A polarization-independent isolator (PI-ISO) is placed between EDF and PC in the cavity to ensure the unidirectional operation of the pulse light. An optical coupler (OC), with a 10% output, is adopted to direct the laser pulses from the cavity. Furthermore, the characteristics of light pulses generated are measured by an optical spectrum analyzer (Yokogawa AQ6370D) with a resolution of 0.02 nm, a real-time high-speed oscilloscope (Tektronix TBS1102) with a 100-MHz bandwidth, and an autocorrelator (Femtochrome Research, Inc., FR-103MN autocorrelator).

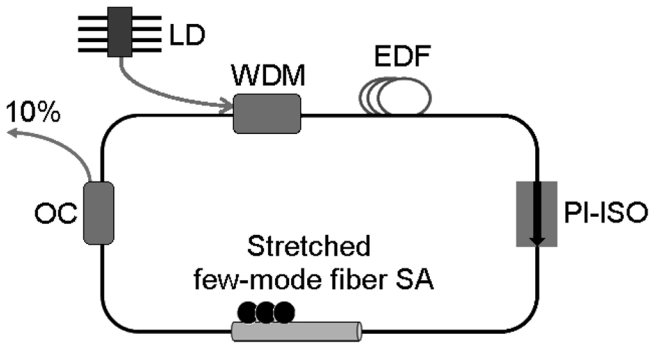

Fig. 2. Schematic of MLFL.

4. Results and Discussion

First, we built an MLFL with a coiled and tapered FMFPC, with a length of 40 cm. The diameter of FMF is tapered from 125 to 110 μm in the experiment, carefully adjusting the orientation of PC; thus, the stable conventional soliton operation is achieved under a pump power of 370 mW. Compared with splicing SIMF (NCF ahead of GIMF), the use of FMF to produce an ultrashort pulse can reduce the insertion loss and increase the nonlinearity of the cavity, assuming that this type of SA has a high damage threshold, with potential applications in high-energy ultrashort pulse generation. The results of the conventional soliton are summarized in Fig. 3. The emergence of symmetrically Kelly sidebands on the spectrum clearly indicates that the MLFL is under conventional soliton operation; see Fig. 3 a. The spectral central wavelength and 3 dB optical spectrum bandwidths are 1588.2 and 4.04 nm, respectively. Using a digital oscillator, we record a pulse train with equal intensity and an even pulse interval of ∼40.7 ns corresponding to the length of the cavity; see Fig. 3 b. The even pulse intensity and interval imply that the mode-locking state is highly stable. A pulse duration of 845 fs is measured by the autocorrelator, using Sech^2 pulse profile fitting; see Fig. 3 c. The time-bandwidth multiple is estimated to be 0.406, assuming that the ultrafast pulse formed is similar to the Sech^2 pulse profile in the time domain.

The radio frequency spectrum is used to verify the stability of the pulse fiber laser; see Fig. 4 a. The fundamental repetition rate (RF) centered at ∼24.52 MHz is consistent with a pulse-to-pulse delay of 40.7 ns. A signal-to-noise ratio (SNR) of 65 dB is obtained with a resolution of 20 kHz and a bandwidth of 40 MHz, indicating that the fiber laser maintains a stable mode-locking operation. Also, we measure the RF spectrum of the 500 MHz span with a radio bandwidth of 20 kHz; see Fig. 4 b. No modulation

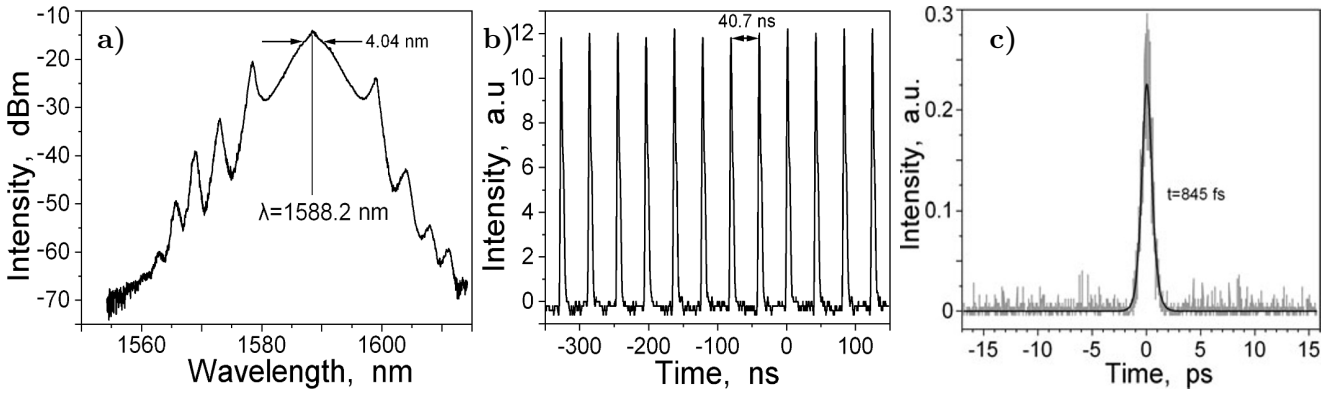

Fig. 3. The performance of conventional soliton with coiled and tapered FMFPCSA in the cavity. Here, the optical spectrum (a), the digital oscillator (b), and the autocorrelation trace (c).

on the harmonics is observed, indicating that the mode-locking state is at the stage of pure single-pulse operation, and the all-fiber MLFL is becoming more stable. Once the pump power threshold is reached by adjusting the proper state of the PC, the self-started mode-locking operation can be achieved. If the experimental environment (including temperature, noise, and other factors) remains unchanged, the mode-locking state lasts for one week.

The fiber laser produces different outputs based on the pump power, as predicted by [30]. The average output power of the fiber laser is recorded as a function of the pump power; see Fig. 5. The maximum output power is 7.4 mW at a pump power of 700 mW. At 360 – 700 mW, the fiber laser is under the continuous mode-locking (CW-ML) operation. At 140 – 360 mW, the fiber laser operates in a Q-switch mode-locked (QS-ML) regime, where the pulse train envelope changes. As the incident pump power increases, the pulse interval in the QS-ML state varies. In Fig. 6, we present the QS-ML results at 140, 200, and 360 mW. Throughout the experiment, the spectrum remains nearly unvaried.

We evaluate the long-term stability of mode-locked pulse generation by monitoring the output spectra of the fiber laser, using the 40 cm length of tapered FMF every 30 min for 270 min. As presented in Fig. 7, the measured spectral center wavelength and spectral bandwidth are unvaried; only a small floatation

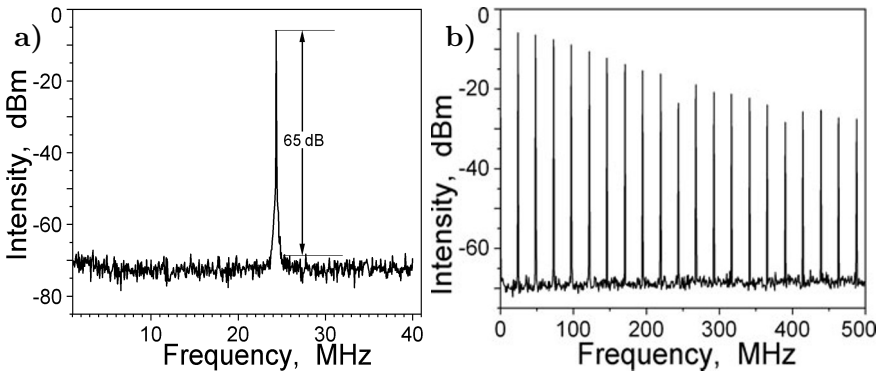

Fig. 4. Typical RF spectrum of the fundamental repetition rate with a span of 40 MHz and a resolution bandwidth of 20 kHz (a) and the RF spectrum with a large bandwidth of 500 MHz and a resolution of 20 kHz (b).

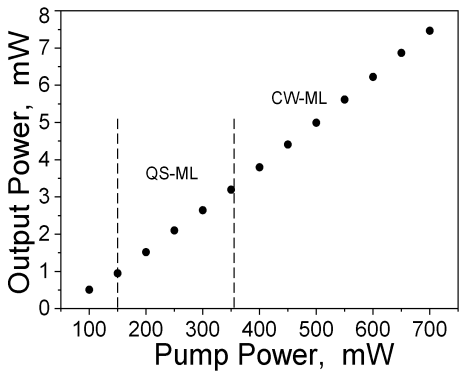

Fig. 5. Output power of the elaborated fiber laser versus the pump power.

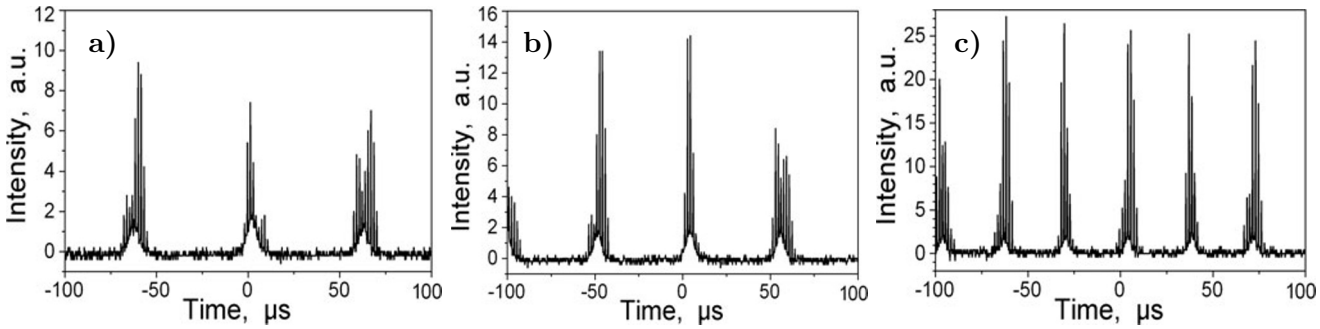

Fig. 6. Laser output in the Q-switched mode-locked state at pump powers of 140 mW (a), 200 mW (b), and 360 mW (c).

exists in the sidebands, within the acceptable error range. These results imply that the MLFL is highly stable.

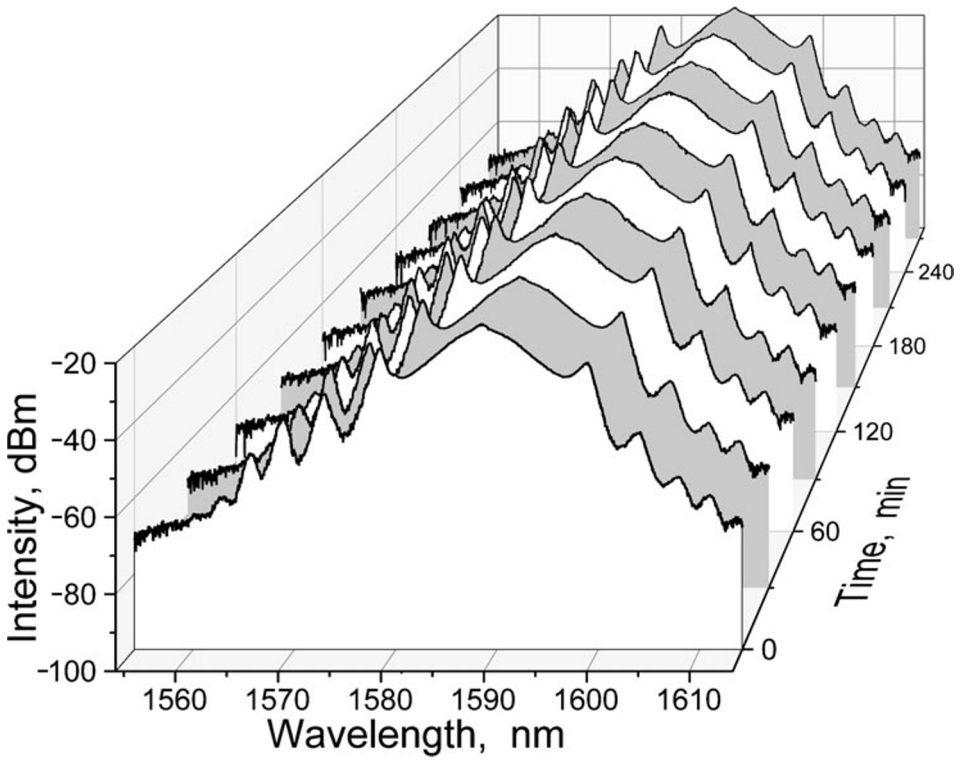

Fig. 7. Long-term stability of the fiber laser elaborated.

In order to study the influence of tapered FMF on mode-locked pulse performance, we replace the tapered FMF with the same length of FMF, without processing in the fiber laser. In Fig. 8 a, we present the spectrum of a mode-locked pulse based on the coiled FMF PC. The center wavelength is 1604.9 nm, and the 3 dB spectrum bandwidth is equal to 4.03 nm. The noticeable presence of Kelly sidebands reveals that the fiber laser operates in an anomalous dispersion regime. The pulse train, pulse duration, and frequency spectrum are measured by an oscilloscope, autocorrelator, and spectrum analyzer; see Fig. 8 b–e.

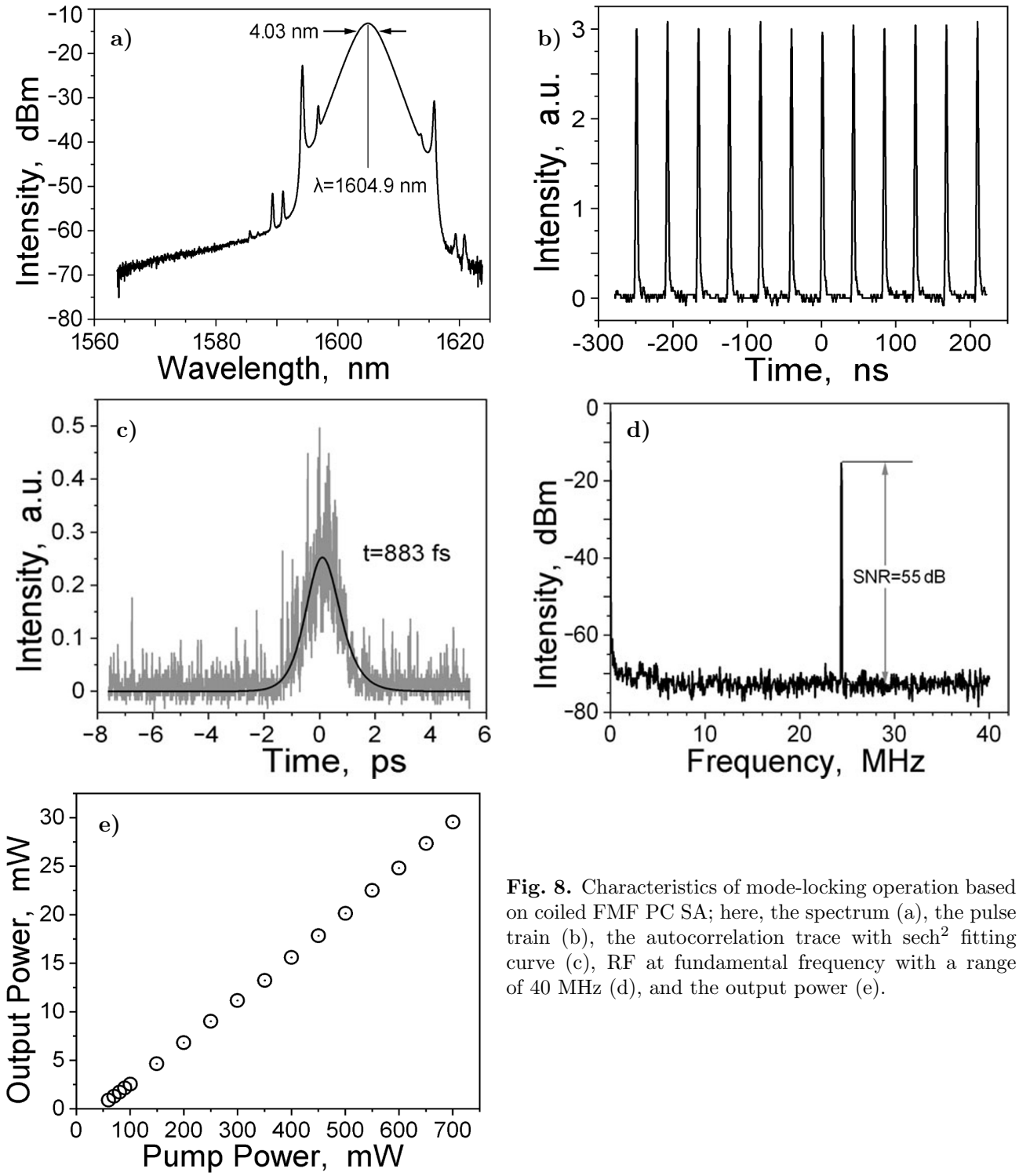

Fig. 8. Characteristics of mode-locking operation based on coiled FMF PC SA; here, the spectrum (a), the pulse train (b), the autocorrelation trace with sech^2 fitting curve (c), RF at fundamental frequency with a range of 40 MHz (d), and the output power (e).

The pulse duration of the mode-locked pulse is approximately 883 fs as measured by an autocorrelation trace, using the $Sech^2$-type function, slightly broader than shown in Fig. 3 c. Introducing the tapered FMF SA can improve the performance of the mode-locked pulse. Figure 8 d reveals an SNR of 55 dB, lower than the 10 dB in Fig. 4 a. Consequently, the coiled and tapered FMF PC SA is more stable in an MLFL. In Fig. 8 e, we present the output power with the unprocessed FMF; it is higher than that of the tapered FMF because of the processed FMF. The diameter of the FMF is tapered from 125 to 110 μm, causing light to leak out and create an evanescent field.

5. Conclusions

In this paper, we proposed, elaborated, and demonstrated the SA based on a coiled and tapered graded-index FMF PC for a passive MLFL. The output mode-locked pulses had a central wavelength of 1588.2 nm, a 3 dB spectral width of 4.04 nm, and a pulse duration of 845 fs at a fundamental repetition rate of 24.52 MHz, with an SNR of 65 dB. The pulse width was shorter and the SNR was higher than FMF without processing, indicating that the MLFL had higher performance and operation stability. Furthermore, QS-ML was observed in the experiment. As the pump power increased, a transition from QS-ML to a stable CW-ML operation was observed. A coiled and tapered FMF PC as an efficient SA in the elaborated fiber laser suggested that an all-fiber mode-locked laser could have a wide range of practical applications in ultra-wide spectrum formation, spectroscopy, and optical amplifier seeding.

Acknowledgments

This research is supported by the Natural Science Foundation of Fujian Province under Grant No. 2023J01952, Fujian Education Department Funds under Grant No. JAT200355, the Research Foundation of Fujian University of Technology under Grant No.GY-Z20163, the National Natural Science Foundation of China under Grant No. 12005039, and the Natural Science Foundation of Fujian Province under Grant No. 2021J011078. We thank Philip Pape, PhD from Edanz Agency (`www.edanz.com/ac`) for editing a draft of this manuscript.

References

1. H. Zhang, Q. Bao, D. Tang, and L. Zhao, *Appl. Phys. Lett.*, **95**, 141103 (2009).
2. F. W. Wise, A. Chong, and W. H. Renninger, *Laser Photon. Rev.*, **2**, 58 (2008).
3. T. X. Wang, Z. J. Yan, Q. Q. Huang, and C. H. Zou, *IEEE J. Sel. Top. Quantum Electron.*, **24**, 1 (2017).
4. U. Keller and K. J. Weingarten, *IEEE J. Sel. Top. Quantum Electron.*, **2**, 435 (1996).
5. Y. Y. Luo, L. Lei, L. Zhao, and Q. Sun, *IEEE Photonics J.*, **8**, 1 (2017).
6. Y. Meng, Y. Li, Y. Xu, and F. Wang, *Sci. Rep.*, **7**, 45109 (2017).
7. D. Li, H. Jussila, Y. Wang, and G. Hu, *Sci. Rep.*, **8**, 2738 (2018).
8. H. Ahmad, F. D. Muhammad, M. Z. Zulkifli, and S. W. Harun, *IEEE Photonics J.*, **5**, 1501709 (2013).
9. H. Zhang, D. Y. Tang, L. M. Zhao, and Q. L. Bao, *Laser Phys. Lett.*, **7**, 591 (2010).
10. C. Li, J. H. Chen, S. C. Yan, and F. Xu, *IEEE Photonics J.*, **8**, 1500307 (2017).
11. X. X. Jin, G. H. Hu, M. Zhang, et al., *Opt. Express*, **26**, 12506 (2018).
12. J. Sotor, G. Sobon, W. Macherzynski, and P. Paletko, *Appl. Phys. Lett.*, **107**, 440 (2015).
13. L. Yun, *Opt. Express*, **25**, 32380 (2017).
14. D. Mao, S. Zhang, Y. Wang, and X. Gan, *Opt. Express*, **23**, 27509 (2015).

15. P. G. Yan, *Opt. Mater. Express*, **5**, 479 (2015).
16. H. Chen, J. D. Yin, J. W. Yang, and X. J. Zhang, *Opt. Lett.*, **42**, 4279 (2017).
17. E. Nazemosadat and A. Mafi, *J. Opt. Soc. Am. B.*, **30**, 1357 (2013).
18. Z. K. Wang, D. N. Wang, F. Yang, and L. J. Li, *J. Lightw. Technol.*, **35**, 5280 (2017).
19. U. Tegin and B. Ortac, *Opt. Lett.*, **43**, 1611 (2018).
20. H. H. Li, Z. K. Wang, C. Li, and J. J. Zhang, *Opt. Express*, **25**, 26546 (2017).
21. F. Y. Zhao, Y. S. Wang, H. S. Wang, and X. H. Hu, *Sci. Rep.*, **8**, 16369 (2018).
22. F. Y. Zhao, H. S. Wang, Y. S. Wang, and X. H. Hu, *Laser Phys.*, **28**, 085104 (2018).
23. T. Y. Zhu, A. K. Wang, D. N. Wang, and F. Yang, *Photonics Res.*, **7**, 853 (2019).
24. Z. K. Wang, J. K. Chen, T. Y. Zhu, and D. N. Wang, *Photonics Res.*, **7**, 1214 (2019).
25. S. Thulasi and S. Sivabalan, *IEEE Photonics Technol. L.*, **99**, 1 (2021).
26. B. F. Zhao, J. Guo, Q. R. He, and S. C. Ma, *Chin. Opt. Lett.*, **20**, 041403 (2022).
27. X. Li, D. N. Wang, and J. K. Chen, *J. Opt. Soc. Am. B.*, **38**, 2112 (2021).
28. N. M. Jin, D. N. Wang, S. L. Cai, and Y. Q. Peng, *Laser Phys. Lett.*, **20**, 065102 (2023).
29. X. F. Wang, G. Farrell, E. Lewis, and T. Ke, *J. Lightw. Technol.*, **35**, 4087 (2017).
30. C. Honninger, R. Paschotta, F. Morier-Genoud, and M. Moser, *J. Opt. Soc. Am. B.*, **16**, 46 (1999).